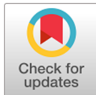

Research Article | Vol. 25, No. 15 | 24 Jul 2017 | OPTICS EXPRESS 18058

Optics EXPRESS

Monolithically-integrated distributed feedback laser compatible with CMOS processing

EMIR SALIH MAGDEN,[1,*] NANXI LI,[1,2] PURNAWIRMAN,[1] JONATHAN D. B. BRADLEY,[1,3] NEETESH SINGH,[1] ALFONSO RUOCCO,[1] GALE S. PETRICH,[1,4] GERALD LEAKE,[5] DOUGLAS D. COOLBAUGH,[5] ERICH P. IPPEN,[1] MICHAEL R. WATTS,[1] AND LESLIE A. KOLODZIEJSKI[1]

[1]*Research Laboratory of Electronics, Massachusetts Institute of Technology, 77 Massachusetts Ave., Cambridge, MA 02139, USA*
[2]*John A. Paulson School of Engineering and Applied Science, Harvard University, 29 Oxford St., Cambridge, MA 02138, USA*
[3]*Department of Engineering Physics, McMaster University, 1280 Main St. W., Hamilton, Ontario L8S 4L8, Canada*
[4]*Lockheed Martin, Missiles and Fire Control, Santa Barbara Focalplane, 346 Bollay Dr., Goleta, CA 93117, USA*
[5]*College of Nanoscale Science and Engineering, University at Albany, 1400 Washington Ave., Albany, NY 12203, USA*
[*]*esm@mit.edu*

Abstract: An optically-pumped, integrated distributed feedback laser is demonstrated using a CMOS compatible process, where a record-low-temperature deposited gain medium enables integration with active devices such as modulators and detectors. A pump threshold of 24.9 mW and a slope efficiency of 1.3 % is demonstrated at the lasing wavelength of 1552.98 nm. The rare-earth-doped aluminum oxide, used as the gain medium in this laser, is deposited by a substrate-bias-assisted reactive sputtering process. This process yields optical quality films with 0.1 dB/cm background loss at the deposition temperature of 250 °C, and therefore is fully compatible as a back-end-of-line CMOS process. The aforementioned laser's performance is comparable to previous lasers having gain media fabricated at much higher temperatures (> 550 °C). This work marks a crucial step towards monolithic integration of amplifiers and lasers in silicon microphotonic systems.

© 2017 Optical Society of America

OCIS codes: (130.3120) Integrated optics devices; (140.3500) Lasers, erbium; (310.1860) Deposition and fabrication; (140.3490) Lasers, distributed-feedback.

References and links

1. T. Kitagawa, K. Hattori, M. Shimizu, Y. Ohmori, and M. Kobayashi, "Guided-wave laser based on erbium-doped silica planar lightwave circuit," Electron. Lett. **27**, 334–335 (1991).
2. A. Ortiz, J. Alonso, V. Pankov, A. Huanosta, and E. Andrade, "Characterization of amorphous aluminum oxide films prepared by the pyrosol process," Thin Solid Films **368**, 74–79 (2000).
3. E. D. Palik, *Handbook of Optical Constants of Solids*, vol. 3 (Academic, 1998).
4. Y. Yan, A. Faber, H. de Waal, P. Kik, and A. Polman, "Erbium-doped phosphate glass waveguide on silicon with 4.1 db/cm gain at 1.535 µm," Appl. Phys. Lett. **71**, 2922–2924 (1997).
5. K. Miura, J. Qiu, H. Inouye, T. Mitsuyu, and K. Hirao, "Photowritten optical waveguides in various glasses with ultrashort pulse laser," Appl. Phys. Lett. **71**, 3329–3331 (1997).
6. Y. Kurokawa, T. Ishizaka, T. Ikoma, and S. Tero-Kubota, "Photo-properties of rare earth ion (Er^{3+}, Eu^{3+} and Sm^{3+})-doped alumina films prepared by the sol-gel method," Chemical physics letters **287**, 737–741 (1998).
7. J. D. Bradley and M. Pollnau, "Erbium-doped integrated waveguide amplifiers and lasers," Laser Photon. Rev. **5**, 368–403 (2011).
8. R. Soulard, A. Zinoviev, J. Doualan, E. Ivakin, O. Antipov, and R. Moncorgé, "Detailed characterization of pump-induced refractive index changes observed in $Nd:YVO_4$, $Nd:GdVO_4$ and Nd:KGW," Opt. Express **18**, 1553–1568 (2010).
9. S. A. Vázquez-Córdova, M. Dijkstra, E. H. Bernhardi, F. Ay, K. Wörhoff, J. L. Herek, S. M. García-Blanco, and M. Pollnau, "Erbium-doped spiral amplifiers with 20 dB of net gain on silicon," Opt. Express **22**, 25993–26004 (2014).

#291876 https://doi.org/10.1364/OE.25.018058
Journal © 2017 Received 3 Apr 2017; revised 11 Jul 2017; accepted 12 Jul 2017; published 19 Jul 2017

10. M. Belt and D. J. Blumenthal, "High temperature operation of an integrated erbium-doped DBR laser on an ultra-low-Loss Si_3N_4 platform," in "OFC Technical Digest", (Optical Society of America, 2015), Tu2C.7.
11. N. Li, Z. Su, Purnawirman, E. S. Magden, C. V. Poulton, A. Ruocco, N. Singh, M. J. Byrd, J. D. B. Bradley, G. Leake, and M. R. Watts, "Athermal synchronization of laser source with WDM filter in a silicon photonics platform," Appl. Phys. Lett. **110**, 211105 (2017).
12. E. Bernhardi, H. Van Wolferen, L. Agazzi, M. Khan, C. Roeloffzen, K. Wörhoff, M. Pollnau, and R. De Ridder, "Ultra-narrow-linewidth, single-frequency distributed feedback waveguide laser in Al_2O_3:Er^{3+} on silicon," Opt. Lett. **35**, 2394–2396 (2010).
13. K. Zhang and J. U. Kang, "C-band wavelength-swept single-longitudinal-mode erbium-doped fiber ring laser," Opt. Express **16**, 14173–14179 (2008).
14. Purnawirman, N. Li, E. S. Magden, G. Singh, N. Singh, A. Baldycheva, E. S. Hosseini, J. Sun, M. Moresco, T. N. Adam, G. Leake, D. Coolbaugh, J. D. B. Bradley, and M. R. Watts, "Ultra-narrow-linewidth Al_2O_3:Er^{3+} lasers with a wavelength-insensitive waveguide design on a wafer-scale silicon nitride platform," Opt. Express **25**, 13705–13713 (2017).
15. M Belt, T. Huffman, M. L. Davenport, W. Li, J. S. Barton, and D. J. Blumenthal, "Arrayed narrow linewidth erbium-doped waveguide-distributed feedback lasers on an ultra-low-loss silicon-nitride platform," Opt. Lett. **38**, 4825–4828 (2013).
16. J. H. Wong, H. Q. Lam, S. Aditya, J. Zhou, N. Li, J. Xue, P. H. Lim, K. E. K. Lee, K. Wu, and P. P. Shum, "Photonic generation of frequency-tunable microwave signals using an array of uniformly spaced optical combs," J. Lightw. Tech. **30**, 3164–3172 (2012).
17. N. Li, E. Timurdogan, C. V. Poulton, M. Byrd, E. S. Magden, Z. Su, G. Leake, D. D. Coolbaugh, D. Vermeulen, and M. R. Watts, "C-band swept wavelength erbium-doped fiber laser with a high-Q tunable interior-ridge silicon microring cavity," Opt. Express **24**, 22741–22748 (2016).
18. Y. Song, S. Havstad, D. Starodubov, Y. Xie, A. Willner, and J. Feinberg, "40-nm-wide tunable fiber ring laser with single-mode operation using a highly stretchable FBG," IEEE Photon. Tech. Lett. **13**, 1167–1169 (2001).
19. N. Li, Z. Su, E. S. Magden, P. T. Callahan, K. Shtyrkova, M. Xin, A. Ruocco, C. Baiocco, E. P. Ippen, F. X. Kärtner, J. D. B. Bradley, D. Vermeulen, and M. R. Watts, "High-power thulium lasers on a silicon photonics platform," Opt. Lett. **42**, 1181–1184 (2017).
20. J. Bradley, L. Agazzi, D. Geskus, F. Ay, K. Wörhoff, and M. Pollnau, "Gain bandwidth of 80 nm and 2 dB/cm peak gain in Al_2O_3:Er^{3+} optical amplifiers on silicon," J. Opt. Soc. Am. B **27**, 187–196 (2010).
21. E. S. Hosseini, J. D. Bradley, J. Sun, G. Leake, T. N. Adam, D. D. Coolbaugh, and M. R. Watts, "CMOS-compatible 75 mW erbium-doped distributed feedback laser," Opt. Lett. **39**, 3106–3109 (2014).
22. C. M. Sorace-Agaskar, P. T. Callahan, K. Shtyrkova, A. Baldycheva, M. Moresco, J. Bradley, M. Y. Peng, N. Li, E. S. Magden, P. Purnawirman, M. Y. Sander, G. Leake, D. D. Coolbaugh, M. R. Watts, and F. X. Kärtner, "Integrated mode-locked lasers in a CMOS-compatible silicon photonic platform," in "CLEO: 2015 OSA Technical Digest", (Optical Society of America, 2015), SM2I.5.
23. Purnawirman, N. Li, E. S. Magden, G. Singh, M. Moresco, T. N. Adam, G. Leake, D. Coolbaugh, J. D. B. Bradley, and M. R. Watts "Wavelength division multiplexed light source monolithically integrated on a silicon photonics platform," Opt. Lett. **42**, 1772–1775 (2017).
24. K. Wörhoff, J. D. Bradley, F. Ay, D. Geskus, T. P. Blauwendraat, and M. Pollnau, "Reliable low-cost fabrication of low-loss waveguides with 5.4-db optical gain," IEEE J. Quantum Electron. **45**, 454–461 (2009).
25. A. Franke, D. Bilic, D. Chang, P. Jones, T.-J. King, R. Howe, and G. Johnson, "Post-CMOS integration of germanium microstructures," in "Micro Electro Mechanical Systems, 1999. MEMS'99. Twelfth IEEE International Conference on," (IEEE, 1999), 630–637.
26. H. Takeuchi, A. Wung, X. Sun, R. T. Howe, and T.-J. King, "Thermal budget limits of quarter-micrometer foundry CMOS for post-processing MEMS devices," IEEE Trans. Electron. Dev. **52**, 2081–2086 (2005).
27. S. Sedky, A. Witvrouw, H. Bender, and K. Baert, "Experimental determination of the maximum post-process annealing temperature for standard CMOS wafers," IEEE Trans. Electron. Dev. **48**, 377–385 (2001).
28. H. Z. Durusoy, Ö. Duyar, A. Aydinli, and F. Ay, "Influence of substrate temperature and bias voltage on the optical transmittance of TiN films," Vacuum **70**, 21–28 (2003).
29. E. S. Magden, "Rare-earth doped aluminum oxide lasers for silicon photonics," Thesis, Massachusetts Institute of Technology (2014).
30. E. Bachari, G. Baud, S. B. Amor, and M. Jacquet, "Structural and optical properties of sputtered ZnO films," Thin Solid Films **348**, 165–172 (1999).
31. G. Hirata, N. Perea, M. Tejeda, J. Gonzalez-Ortega, and J. McKittrick, "Luminescence study in eu-doped aluminum oxide phosphors," Opt. Mater. **27**, 1311–1315 (2005).
32. S. Gullapalli, R. Vemuri, F. Manciu, J. Enriquez, and C. Ramana, "Tungsten oxide (WO_3) thin films for application in advanced energy systems," J. Vac. Sci. Technol. **28**, 824–828 (2010).
33. E. Fortunato, A. Pimentel, A. Gonçalves, A. Marques, and R. Martins, "High mobility amorphous/nanocrystalline indium zinc oxide deposited at room temperature," Thin Solid Films **502**, 104–107 (2006).
34. G. Singh, J. D. B. Bradley, N. Li, E. S. Magden, M. Moresco, T. N. Adam, G. Leake, D. Coolbaugh, and M. R. Watts, "Resonant pumped erbium-doped waveguide lasers using distributed bragg reflector cavities," Opt. Lett. **41**, 1189–1192 (2016).

Optics EXPRESS

35. M. Belt and D. J. Blumenthal, "Erbium-doped waveguide DBR and DFB laser arrays integrated within an ultra-low-loss Si_3N_4 platform," Opt. Express **22**, 10655–10660 (2014).

1. Introduction

The use of rare-earth-doped glass media in integrated optics applications has been studied for amplification and generation of light since its first demonstration in 1991 [1]. Of the numerous possible host glasses for rare-earth-dopants, the interest in amorphous aluminum oxide (Al_2O_3) has many reasons. Al_2O_3's higher refractive index than those of similar host media such as silica, phosphate glass, or fluoride glass enables higher integration density of optical components [2–5]. Al_2O_3 also provides good rare-earth ion solubility [6], and is more easily fabricated via physical vapor deposition techniques as compared to crystalline hosts that require epitaxial growth [7]. Moreover, smaller thermal and excitation-induced refractive index changes help provide more stable gain [8–11], making rare-earth-doped Al_2O_3 a potential gain medium with better noise performance than that of III-V semiconductors [12–15]. Wide gain-bandwidth of various rare-earth dopants also help to achieve wavelength tunability and design flexibility throughout their emission spectra [16–19]. Such advantages have led to recent demonstrations of erbium-doped Al_2O_3 ($Al_2O_3:Er^{3+}$) waveguide amplifiers [20], as well as high-power, integrated continuous-wave and pulsed lasers [21–23].

For a waveguide material having such promising gain characteristics, a reliable and robust fabrication process is crucial. So far, the reactive radio frequency (RF) magnetron sputtering in a mainly argon (Ar) environment has been found to be the most reliable due to its relatively high-rate, OH-free deposition on large area substrates. However, although background losses as low as 0.11 dB/cm have been reported in undoped Al_2O_3 films that were deposited with this method, a deposition temperature of 550 °C was required in order to reduce the background loss [24]. Previously, it has been empirically shown that post-processing of CMOS wafers at temperatures over 425 °C to 525 °C can compromise the integrity of the metal contacts and vias by resistance increase and dopant activation [25–27]. This degradation significantly limits the performance of an integrated optical system, where active devices such as modulators, filters, and detectors inherently require low-resistance contacts for high-speed operation. Therefore, for full monolithic integration of CMOS and photonic structures on the same die, it is essential to develop a deposition procedure that can reliably yield low loss Al_2O_3 films at lower temperatures within CMOS post-processing thermal budgets. One way to improve the sputtered film quality is to use a substrate bias, where the substrate is bombarded by Ar^+ ions during deposition. This technique has been shown to enhance optical transmission, and improve film surface quality for other dielectrics such as TiN [28]. However, the effect of substrate bias on the Al_2O_3 film quality at CMOS-compatible temperatures has not been studied prior to this work.

In this paper, we first investigate how the application of a substrate bias can compensate for the reduced deposition temperatures for reactively sputtered Al_2O_3. We determine the optimum fabrication parameters that yield the Al_2O_3 film with the lowest optical propagation loss, while still maintaining backend CMOS-compatibility. Using these parameters, we then fabricate and characterize $Al_2O_3:Er^{3+}$ films for use in active photonics devices. Finally, we design, fabricate, and characterize a distributed feedback (DFB) laser that uses the newly developed $Al_2O_3:Er^{3+}$ as its gain medium.

2. Material development and optimization

The $Al_2O_3:Er^{3+}$ gain medium was deposited using a Kurt J. Lesker Lab 18 thin film sputtering system with magnetron sputtering guns and RF power supplies. The system was consistently kept under vacuum with a base pressure of 10^{-7} Torr; and samples were loaded with the use of a load lock. The ability to separately control the target and substrate shutters allowed for a

Optics EXPRESS

more reliable deposition process, yielding films with consistent quality and thickness. First, the undoped Al_2O_3 film was studied. The films were reactively sputtered from an Al target with 99.999 % purity in an Ar/O_2 environment of 3 mT process pressure as regulated primarily by the Ar flow rate. O_2 was separately introduced and the flow rate was kept around 4.0 - 4.3 sccm, after which the bias voltage on the Al target started to decrease significantly [29]. This allowed for high deposition rates (5 - 6 nm/min) of optical quality, stoichiometric Al_2O_3, without fully oxidizing the Al target. With this O_2 flow, an RF power of 400 W was applied to the Al target, resulting in a bias voltage of 210 V.

The optical quality of the sputtered Al_2O_3 films was characterized using a Metricon 2010/M prism coupling system with lasers at 633 nm, 829 nm, and 1550 nm. Film thickness, index, and propagation losses were measured using slab waveguides formed by 1 μm thick Al_2O_3 films deposited on thermally oxidized Si/SiO_2 substrates. The thermal oxide thickness was 6 μm. To obtain the optimum deposition parameters for the best optical quality Al_2O_3, a set of depositions was performed at temperatures ranging from 125 °C to 450 °C, and with substrate biases ranging from 0 W to 90 W.

Films with the lowest optical losses were obtained at an optimum temperature of approximately 250 °C [Fig. 1(a)], and with the highest possible substrate bias of 90 W [Fig. 1(b)]. The measured propagation loss in the Al_2O_3 film using these ideal parameters was as low as 0.1 dB/cm at 1550 nm where the refractive index was $n_{Al_2O_3} = 1.578$. At temperatures significantly below or above 250 °C, or with a smaller substrate bias, propagation losses over 10 dB/cm were measured. At lower temperatures and insufficient substrate biases, the increased loss can be explained by the reduced surface mobility, which is known to cause clusters and voids in the deposited layer [24]. This is corroborated by the surface roughness measurements from films that were deposited with 0 W and 90 W of substrate biases at a temperature of 250 °C. According to the atomic force micrograph in Fig. 1(c), for the film deposited without a substrate bias, a root mean square roughness (R_q) of 3.34 nm is obtained over a 1 μm^2 area; and a rough surface morphology is observed. In contrast, when 90 W of substrate bias is used, the surface roughness is reduced by almost an order of magnitude to $R_q = 0.35$ nm, providing a much smoother surface that can help achieve lower propagation losses [Fig. 1(d)]. For films deposited at temperatures higher than 250 °C, the root mean square roughness R_q remained below 0.6 nm, indicating no significant contribution to the observed optical losses. The increased losses can be explained by the enhanced surface mobility of the sputtered film [30], which can lead to formation of Al_2O_3 nanocrystals. Previously, nanocrystalline structure formation has been observed at temperatures much below those required for poly- or single-crystalline formation. Examples include nanocrystals synthesized at 280 °C for aluminum europium oxide ($(Al_{1-x}Eu_x)_2O_3$) [31], and sputtered at 200 °C and room temperature for tungsten oxide [32] and indium zinc oxide [33] respectively. Consequently, the application of substrate bias in combination with an increasing deposition temperature above 250 °C can lead to nanocrystal formation in the sputtered Al_2O_3 films. Increased optical losses at higher temperatures can be attributed to scattering from these nanoscale boundaries.

Once the optimum deposition parameters have been determined for the undoped Al_2O_3, doped films were fabricated by means of co-sputtering where an Er and an Al target were simultaneously sputtered. The concentration of Er^{3+} ions was controlled by the bias voltage across the Er target during fabrication. The background loss and Er^{3+} concentration in the doped films were modeled according to

$$\alpha(\lambda) = \alpha_0 + 10\log(e)\,\sigma_{abs}(\lambda)\,\Gamma N_0, \tag{1}$$

where $\alpha(\lambda)$ is the total absorption, α_0 is the background absorption due to scattering, $\sigma_{abs}(\lambda)$ is the absorption cross-section, Γ is the mode confinement factor within the Al_2O_3:Er^{3+} layer, and N_0 is the number of dopant ions per unit volume. Here, α_0 and Γ are assumed to be wavelength independent within the measurement window of 1505 nm - 1575 nm. Shown in Fig. 2(a) are

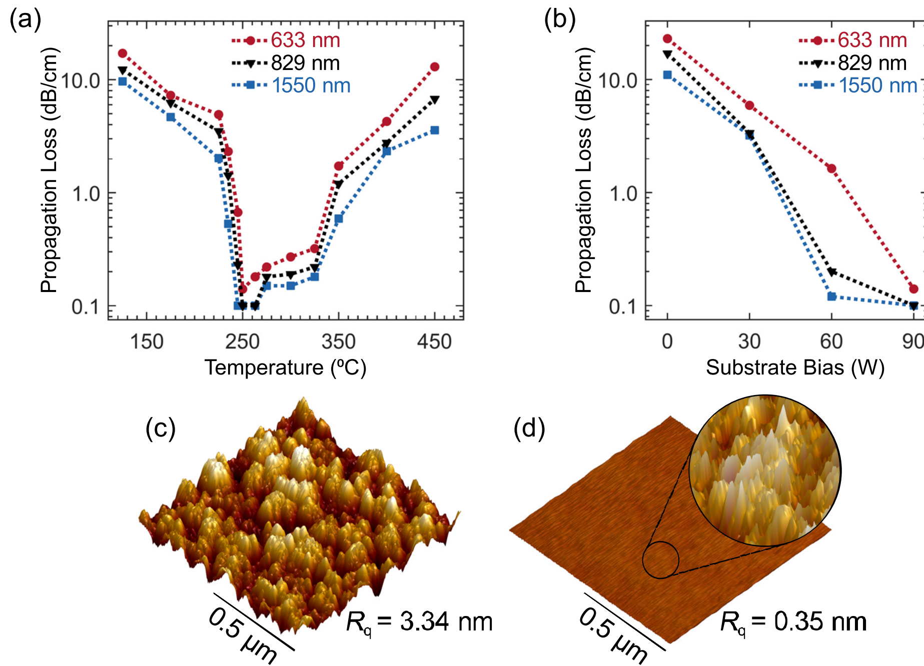

Fig. 1. Propagation loss as a function of (a) deposition temperature, and (b) substrate bias for 1 μm thick Al_2O_3, where the optimum quality is achieved at 250 °C and 90 W. Atomic force micrographs for films deposited with (c) 0 W and (d) 90 W substrate bias with significant difference in surface texture. Inset shows the profile of a smaller area from the smoother film with the 90 W bias, where the vertical scale is enhanced by 15 times.

the absorption results as functions of wavelength for two films with erbium target voltages of V_{Er} = 75 V and V_{Er} = 60 V, as measured by the prism coupling method. In this measurement, light from an Agilent 81600B tunable laser source was coupled through a rotating prism to the slab modes in Al_2O_3 films sputtered on Si/SiO_2 substrates. The loss was characterized at each wavelength from the decay of the scattered light intensity along the propagation direction, as measured from a fiber mounted on a motorized stage. Background intensity was subtracted by setting the reading offset to zero when the incident light was turned off. The recorded intensity as a function of propagation length was then analyzed using an exponential fit. In the 1505 nm - 1575 nm wavelength range, the error in the exponential fits remained below ± 0.1 dB/cm.

In order to determine N_0 and α_0, the absorption is replotted in Fig. 2(b) as a function of $\sigma_{abs}(\lambda)$, which was previously reported in [24] by Wörhoff et al. Then, according to the model in Eq. (1), each dataset is analyzed with a linear fit, yielding dopant concentrations of $N_{0,75V} = 1.9 \times 10^{20}\,cm^{-3}$ and $N_{0,60V} = 9.5 \times 10^{19}\,cm^{-3}$ for V_{Er} = 75 V and V_{Er} = 60 V respectively. Background losses on the order of 0.1 dB/cm were reliably achieved at both concentrations, as indicated by the vertical intercepts of the linear fits in Fig. 2(b).

3. Laser design and characterization

After the spectral properties of the newly developed $Al_2O_3:Er^{3+}$ films were characterized, this gain material was used to design an optically-pumped, quarter-wave phase shifted DFB laser. With the exception of the sputtered $Al_2O_3:Er^{3+}$ gain medium, the laser was fabricated in a 300 mm CMOS foundry. The fabrication procedure is illustrated in Fig. 3. First, a 6 μm thick layer of SiO_2 and a 200 nm thick layer of SiN were deposited by plasma-enhanced chemical

Optics EXPRESS

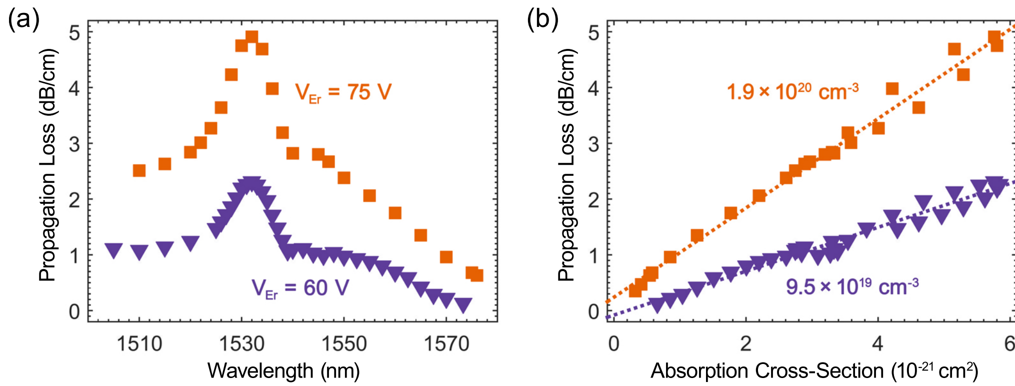

Fig. 2. Total absorption measured in deposited films with 75 V and 60 V bias across the Er target with respect to (a) wavelength and (b) absorption cross-section. Background loss and dopant concentrations are calculated by linear fits.

vapor deposition (PECVD) [Fig. 3(a)]. In order to minimize absorption losses, the plasma conditions were optimized for a low hydrogen content in the deposited layers, while maintaining a high refractive index for the SiN. SiO_2 and the SiN layers were both chemically-mechanically polished (CMP) in order to achieve the accurate final thicknesses, and to reduce scattering losses due to surface roughness. The SiN layer was then patterned using 193 nm immersion lithography and reactive ion etching, creating the waveguide and feedback structures, and the quarter-wave phase shift in Fig. 3(b). After the SiN layer, a thin layer of SiO_2 was deposited using PECVD, for which a final thickness of 100 nm was achieved using CMP [Fig. 3(c)]. Finally, large trenches were etched on the die borders for fiber coupling. After the wafers were diced, the $Al_2O_3:Er^{3+}$ gain medium was deposited as a back-end process [Fig. 3(d)], using the techniques described above.

The laser was designed using the fundamental modes for both the pump and signal, in order to achieve maximum overlap within the gain medium, and to avoid any potential losses that would be observed by any higher order modes. The goal of the segmented SiN design detailed in Fig. 4 is to achieve high confinement and overlap of the fundamental transverse electric (TE) signal and pump modes within the gain medium. Compared to a single wider segment, multiple segments of SiN allow the fundamental TE modes to achieve good overlap with the gain medium, while still being laterally confined. These confinement and overlap factors are optimized with the design shown in Fig. 4(a), where the width of each SiN segment is w_{SiN} = 450 nm, and they are separated from each other by a gap of g_{SiN} = 400 nm. The thickness of the SiN layer and

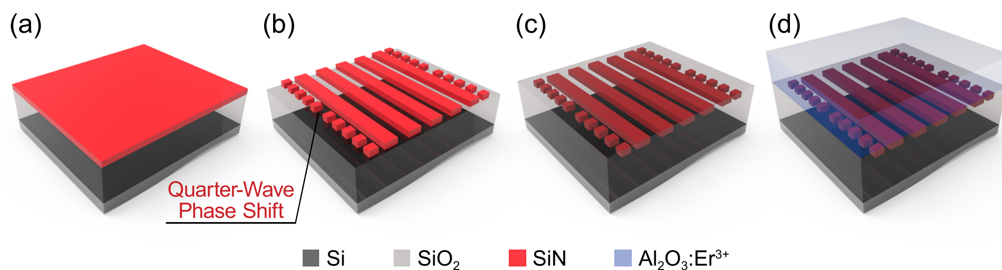

Fig. 3. Fabrication procedure for quarter-wave phase shifted DFB laser where the grating is defined in the buried SiN, and the $Al_2O_3:Er^{3+}$ is blanket-deposited as a back-end-of-line CMOS-compatible process.

Optics EXPRESS

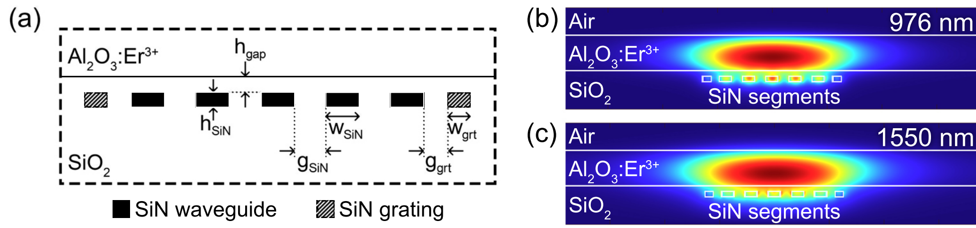

Fig. 4. (a) Cross-section of laser cavity showing the buried SiN waveguide and grating segments (not to scale). Fundamental TE modes of (b) 980 nm pump and (c) 1550 nm signal in the laser cavity.

the vertical spacing from the gain medium are $h_{SiN} = 200\,nm$ and $h_{gap} = 200\,nm$, as dictated by the CMOS fabrication process. The nominal thickness of the deposited $Al_2O_3:Er^{3+}$ layer was 1.2 µm, with a radial variation of approximately 5 % from the center to the edge of the 200 mm substrate holder. Using these design parameters, the field profiles for the fundamental TE modes at the pump and signal wavelengths are simulated, as shown in Fig. 4(b) and 4(c). The gain medium confinement of the pump and signal modes are calculated to be $\Gamma_p = 0.841$ and $\Gamma_s = 0.828$ respectively. The intensity overlap of these two modes in the gain medium is $\gamma = 0.903$. This high overlap is enabled by the segmented SiN design, as it allows the shorter wavelength pump mode to expand into the gain medium, which is otherwise mainly confined in the nitride layer in a single segment design. The pump-signal overlap γ is reduced when using the transverse magnetic (TM) mode for either the signal or the pump. Also, since the TM modes in this design can potentially suffer from coupling to substrate modes, more cavity losses would be expected. Therefore due to their larger overlap factor and reduced in-cavity losses, fundamental TE signal and pump modes can provide the largest possible gain per unit length.

Feedback is provided by the buried SiN grating of width $w_{grt} = 300\,nm$ on either side of the waveguide segments. The grating is separated from the adjacent waveguide segment by a gap of $g_{grt} = 300\,nm$. The grating strength is determined by how strongly the signal mode interacts with the grating, and is calculated as $\kappa = 7.56\,cm^{-1}$ between the forward and backward traveling modes in the 1.5 cm long laser cavity. Grating duty cycle was chosen to be 50 %. The grating period is calculated from the Bragg condition given by $\Lambda = \lambda_0/2n_{eff}$ at the signal wavelength of $\lambda_0 = 1550\,nm$. Considering the $Al_2O_3:Er^{3+}$ thickness variation, the period was varied from $\Lambda = 490\,nm$ to 496 nm, in order for the laser to operate within the 1530 nm - 1565 nm C-band.

The integrated laser is characterized using the setup shown in Fig. 5(a). 976 nm fiber-coupled pump diodes were used with polarization controllers to pump the on-chip laser from both sides. Single-mode cleaved fibers were used to couple the pump and signal light on and off chip. The laser emission was collected by a fiber wavelength division multiplexer, and recorded using an optical spectrum analyzer. Using 220 mW of total on-chip pump power, a single-mode signal output of 2.6 mW is recorded at 1552.98 nm, where the emission spectrum is given in Fig. 5(b). The output here is measured with a spectral resolution of 50 pm, the smallest available on a Yokogawa AQ6375 optical spectrum analyzer. No output above the noise floor is measured at any other wavelengths, as expected from the quarter-wave phase shifted DFB design. Moreover, the output wavelength matches well with the design target of 1550 nm for the TE signal mode, indicating the single-mode TE output from the fabricated laser. This performance was achieved with an Er^{3+} doping concentration of $N_0 = 1.2 \times 10^{20}\,cm^{-3}$. Next, the laser performance is evaluated by measuring the output power at the signal wavelength as a function of pump power. The response plotted in Fig. 5(c) was recorded with the optimum pump polarization, corresponding once again to the maximum intensity overlap γ expected with TE pump and signal modes. The pump threshold was measured to be $P_{th} = 24.9\,mW$. With increasing pump

Optics EXPRESS

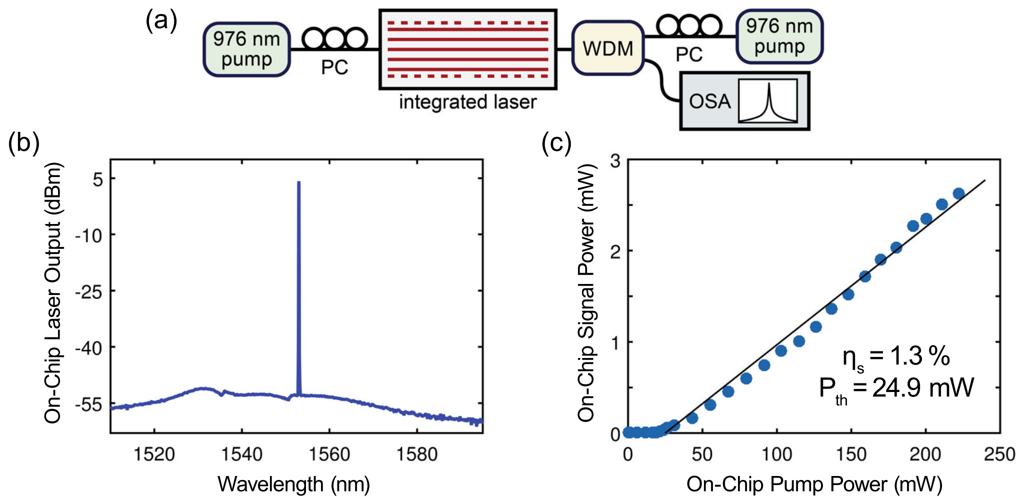

Fig. 5. (a) Experimental setup for characterizing the on-chip laser pumped using a polarization controller (PC), a wavelength division multiplexer (WDM), and measured with an optical spectrum analyzer (OSA). (b) Laser emission spectrum as measured by the OSA. (c) Laser performance characterization as a function of pump power.

power over the threshold, the laser operated with a slope efficiency of $\eta_s = 1.3\,\%$. These results indicate similar performance to lasers whose gain media are fabricated at temperatures over 550 °C [34, 35], demonstrating the functionality of the newly developed 250 °C fabrication process for the Al_2O_3:Er^{3+} gain medium. Potential improvements in both the threshold and the slope efficiency can be achieved by improving pump coupling losses, or by recycling the residual pump back into the laser cavity.

4. Conclusion

We have demonstrated a substrate-bias-assisted sputtering method for the fabrication of undoped and rare-earth-doped Al_2O_3 thin films. The substrate bias allows for backend CMOS-compatible deposition temperatures as low as 250 °C. This makes it possible to integrate amplifiers and lasers with other active silicon photonic devices such as modulators, filters, and detectors that rely on low-resistance metal contacts and vias for high speed operation. Additionally, other rare-earth-dopants such as neodymium, ytterbium, thulium, or holmium can also be co-sputtered with the 250 °C Al_2O_3 film. These dopants can be used in creating amplifiers and lasers at various near-to-mid infrared wavelengths for new applications. This marks an important step towards electronic-photonic integration for communications applications.

Funding

Defense Advanced Research Projects Agency (DARPA) (HR0011-12-2-0007).

Acknowledgments

The authors would like to thank Dr. Josh Conway for useful discussions. N. Li acknowledges a fellowship from Agency of Science, Technology and Research (A*STAR), Singapore.